25 May 2001

ELSEVIER

Chemical Physics Letters 340 (2001) 62–70

CHEMICAL PHYSICS LETTERS

www.elsevier.nl/locate/cplett

$OH(v) + O_3$: Does chemical reaction dominate over non-reactive quenching?

A.J.C. Varandas *, L. Zhang

Departamento de Química, Universidade de Coimbra, P-3049 Coimbra Codex, Portugal

Received 19 December 2000; in final form 23 March 2001

Abstract

We discuss the title atmospheric reaction for vibrational excited states of OH over the range $0 \leqslant v \leqslant 9$. All calculations have employed the quasi-classical trajectory (QCT) method and a realistic double many-body expansion (DMBE) potential energy surface for HO_4 (^2A). For $v = 9$, the calculated thermal rate coefficient is found to agree with measurements of OH quenching reported by others, which has been attributed to both chemical reaction and non-reactive collisions. The temperature dependence of the rate constant is described by a simple model for all studied vibrational states of OH.

1. Introduction

The fate of vibrationally excited OH radicals is important to understand the night sky airglow [1–4]. They are produced by the chemical reaction [5], and references therein)

$$H + O_3 \rightarrow OH(v \leqslant 9) + O_2 \quad (1)$$

with OH controlling the chain reactions occurring in the stratosphere. Because the reactivity of OH depends on its vibrational state, it is important to know the associated microscopic rate constants to monitor atmospheric phenomena and create models of atmospheric chemistry and kinetics. Once produced, $OH(v)$ radicals either fluoresce or undergo deactivation in collisions with the ambient species. Specifically, if the colliding partners are O_2 or O_3, their removal may undergo either through bimolecular de-excitations or reactions. In the case of $OH(v') + O_2(v'')$, recent theoretical studies [6,7] have shown that a very significant fraction of such collisions occur reactively, leading mostly to $O_3^\star$ when $v' = 9$ and $v'' > 13$ (the star indicates that many of such molecules have a vibrational excitation energy above dissociation, although they ultimately lead to stable ozone molecules via vibrational relaxation or dissociation followed by three-body recombination). Thus, such a reaction has been advocated [6,7] as a potential source of ozone in the stratosphere. The issue of reactivity remains unclear though in the case of O_3, and an answer will be attempted in this Letter by focusing on vibrational levels of OH over the range $0 \leqslant v \leqslant 9$, which are the most abundant natural states.

Significant effort has been made over the past decade to measure the vibrational level dependence of the total $OH(v)$ removal rate constants for collisional processes in the laboratory [8–17].

* Corresponding author. Fax: +351-39-827-703.

E-mail address: varandas@qtvs1.qui.uc.pt (A.J.C. Varandas).

0009-2614/01/$ - see front matter
PII: S0009-2614(01)00364-5

Despite being a major constituent of the atmosphere, not much work has been carried out though using O_3 as the colliding partner [18]. Indeed, the $OH + O_3$ reaction not only influences the steady-state concentration of many trace gases which are important in stratospheric chemistry [19], but is also part of the so-called HO_x catalytic cycle for destruction of ozone in the natural stratosphere [1].

Experimentally, there have been only a few reports on the $OH(v) + O_3$ reaction. Coltharp et al. [20] carried out an extensive study of the influence of vibrational quanta on the $OH + O_3$ interaction. Unfortunately, their results are now suspect because of faulty kinetic analysis of the raw data [5,9,18,21,22] which may have led to gross underestimates. Time-dependent measurements of absolute rate constants were initiated by Greenblatt and Wiesenfeld [9], who have measured the relaxation of $v = 9$ by O_3 and found that O_3 is efficient at removing OH molecules from $v = 9$. However, the available experiments did not monitor products of reaction, and hence the possibility exists that such results may have been misinterpreted: in the absence of measuring reaction products, one cannot prove that there is a chemical reaction at all. This point was raised by Teitelbaum et al. [18] who have reported V–T energy transfer rate constants for the collisional deactivation of $OH(v = 1 \rightarrow 4)$ by O_3 at 300 K. They have used an analytical solution of the master equation for vibrational relaxation of Morse oscillators mixed with an inert gas species. From such an approach, they have been able to extract the rate constant $k_{1,0}^{O_3}$ for the process

$$OH(v = 1) + O_3 \rightarrow OH(v = 0) + O_3 \qquad (2)$$

Moreover, by presupposing that scaling relationships exist between the various rate constants, they managed to extract other $k_{v+1,v}^{O_3}$ rates. In fact, although their data was believed to be valid strictly over the range $v = 0 \rightarrow 4$, they carried out an extrapolation to the ninth vibrational level which is of importance for night sky airglow. The result was $k_{9,8}^{O_3} = 2.3 \times 10^{-10}$ cm^3 molecule^{-1} s^{-1}, with an uncertainty of $\pm 30\%$. Such a result is in striking agreement with the value of $k = 2.0 \times 10^{-10}$ cm^3 molecule^{-1} s^{-1} reported by Greenblatt and Wiesenfeld [9] for $OH(v = 9)$ disappearance in the presence of O_3 at 300 K. On the other hand, it is well established that OH in $v = 0$ does react with O_3. Although this rate constant has a relatively small value [5] of $k = 6.7 \times 10^{-14}$ cm^3 molecule^{-1} s^{-1}, there is no reason of principle why reactivity could not be maintained or even enhanced for vibrationally hot OH radicals. In summary, there may be inconsistencies and disagreements in the literature which can be uncovered only by performing both non-reactive and reactive studies of collisions of $OH(v)$ with ozone based on the same HO_4 potential energy surface. This is the major goal of the current work, where we employ for such a purpose the recently reported [23] (this Letter will be referred hereafter as Letter I) double many-body expansion (DMBE) potential energy surface for the ground electronic state of HO_4, ^2A. For the dynamics calculations we will employ the quasi-classical trajectory (QCT) [24] method which has also been employed in Letter I. Since kinetics studies [23] of the reaction $OH(v = 0) + O_3 \rightarrow HO_2 + O_2$ using the same dynamics approach and potential energy surface yielded rate constants in good agreement with the experimental data, one may have additional confidence for using such tools in studies of vibrationally excited OH. The Letter is organized as follows. Section 2 gives a brief survey of the HO_4 (^2A) DMBE potential energy surface, while the computational method is described in Section 3. The dynamics results are presented and discussed in Section 4, and the major conclusions in Section 5.

2. Potential energy surface

The HO_4 DMBE potential energy surface used in the current work is that described in Letter I. Since perspective views of it have been given elsewhere [23,25], no such plots will be presented here for brevity. Instead, we show in Fig. 1 the calculated minimum energy reaction path for the title reaction. Also indicated in this figure is the energetics of the $OH(v = 0 \rightarrow 9) + O_3(v_1 = 0,\ v_2 = 0,\ v_3 = 0)$ channels; v_1 is the quantum number for the

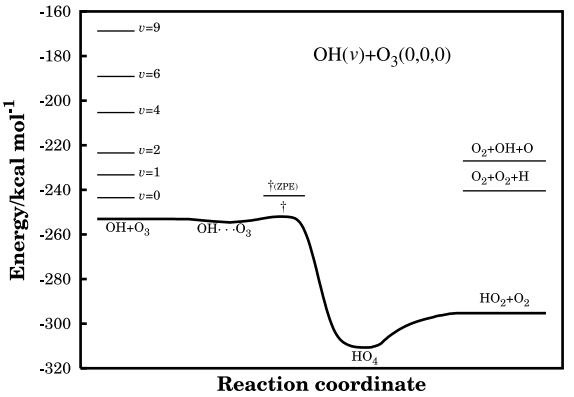

Fig. 1. Minimum energy path for the reaction $OH + O_3 \rightarrow HO_2 + O_2$. The saddle point geometry is indicated by the symbol †, with and without consideration of the corresponding ZPE [7]. Also shown is the energy corresponding to the channels $OH(v = 0 \rightarrow 9) + O_3(v_1 = 0,\ v_2 = 0,\ v_3 = 0)$, $O_2 + O_2 + H$ and $O_2 + OH + O$. For the products, the levels indicate the energies at the equilibrium geometry.

symmetric stretching vibrational normal mode, v_2 for the bending normal mode, and v_3 for the asymmetric stretching normal mode. (Note that in Fig. 3 of [23], the zero-point energy (ZPE) of O_3 has not been included for the level $v = 1$). Clearly, for $v = 2$, the reactive channels leading to $O_2 + O_2 + H$ and $O_2 + OH + O$ are classically feasible even at low translational energies. However, in this energy range, such channels are barely open and hence the problem of ZPE leakage ([26–33], and references therein) may assume special relevance. This issue may not be so crucial for high vibrational quantum numbers of OH ($v \geqslant 4$ or so) due the higher exoergicities involved, a topic which will be further addressed in Section 4.

3. Trajectory calculations

To run the classical trajectories we have utilized the MERCURY/VENUS [24] codes which accommodate the HO_4 DMBE potential energy surface. Calculations have been carried out for $v = 6$ and 9 at diatom–triatom translational energies in the range $1.0 \leqslant E_{tr}/\text{kcal mol}^{-1} \leqslant 16$, as specified in Table 1. These calculations will then be interpreted

Table 1
Summary of trajectory calculations for $OH(v) + O_3$

v	E_{tr} (kcal mol^{-1})	b_{max} (a_0)	N	N_x^r			N^{nr}	$\sigma^r \pm \Delta\sigma^r$ (a_0^2)	$\sigma^{total} \pm \Delta\sigma^{total}$ (a_0^2)
				$x = HO_2^\star + O_2$	$O_2 + O_2 + H$	$O_2 + OH + O$			
6	1	9.83	1000	42	53	18	15	34.28 ± 3.04	38.83 ± 3.20
	2	9.45	1000	40	43	10	23	26.08 ± 2.58	32.53 ± 2.84
	6	7.75	1000	45	45	23	48	21.31 ± 1.89	30.36 ± 2.19
	8	7.75	1000	52	47	22	57	22.82 ± 1.94	33.57 ± 2.28
	12	7.37	1000	65	75	28	78	28.67 ± 2.02	41.98 ± 2.32
9	1	10.20	2000	40	228	77	135	56.43 ± 2.76	78.51 ± 3.12
	2	9.64	3000	69	249	110	234	41.63 ± 1.86	64.39 ± 2.20
	4	8.88	3000	69	270	78	267	34.45 ± 1.56	56.50 ± 1.90
	6	8.32	3000	75	276	108	330	33.23 ± 1.43	57.12 ± 1.75
	8	8.32	3000	75	291	102	372	33.88 ± 1.44	60.82 ± 1.78
	12	7.56	3000	104	420	135	548	39.43 ± 1.36	72.22 ± 1.61
	16	7.37	2000	90	333	116	451	45.99 ± 1.69	84.47 ± 1.91

jointly with the results reported elsewhere [23,25] for lower v states. In all cases the initial rotational quantum number of the colliding OH molecule has been fixed at the ground level ($j = 1$). In turn, the O_3 molecule has been kept in its ground vibrational states ($v_1 = 0,\ v_2 = 0,\ v_3 = 0$), while its rotational energy has been determined by using the microcanonical sampling scheme for a temperature of 300 K. As in Letter I, the determination of the step size for numerical integration, initial diatom–triatom separation, and maximum impact parameter ($b_{\max}$) leading to reaction, have been selected following the usual procedure. Although the outcome of non-reactive collisions will also be examined, such an analysis will be tentative since it is mostly based on parameters optimized for reactive scattering. Batches of typically 2000 trajectories have been carried out for each translational energy, yielding reactive cross-sections ($\sigma^{\mathrm{r}} = \pi b_{\max}^2 (N^{\mathrm{r}}/N)$) with associated 68% uncertainties ($\Delta\sigma^{\mathrm{r}} = ((N - N^{\mathrm{r}})/NN^{\mathrm{r}}))^{1/2}\sigma^{\mathrm{r}}$) smaller than about 10% for most translational energies. A similar methodology has been employed to calculate the non-reactive cross-sections, $\sigma^{\mathrm{nr}} \pm \Delta\sigma^{\mathrm{nr}}$.

Of course, the QCT method suffers from omission of quantum effects, with the problem of ZPE leakage assuming special importance. Both 'active' and 'non-active' fixes have been suggested for this problem ([26–33], and references therein). In the active methods [28–33], a constraint is introduced into the dynamics which prevents the trajectories from entering the region of phase space which would allow the vibrational modes to have less than its ZPE. Instead, in the non-active ones, one simply throws out the trajectories (both reactive and non-reactive) which exhibit unphysical product energies [26], and eventually corrects a posteriori the perturbed statistics [28]. Thus, no further trajectory calculations are required to apply non-active schemes besides those done in the traditional QCT approach. All the above schemes are not free from some ambiguity, and we will use only the simpler non-active methods in Section 4 for illustrative purposes.

From the cross-sections, and assuming a Maxwell–Boltzmann distribution over the translational energy, the specific thermal rate coefficients were obtained as

$$k^{x}(T) = g_{\mathrm{e}}(T)\left(\frac{2}{k_{\mathrm{B}}T}\right)^{3/2}\left(\frac{1}{\pi\mu}\right)^{1/2} \times \int_0^{\infty} E_{\mathrm{tr}}\sigma^{x}\exp\left(-\frac{E_{\mathrm{tr}}}{k_{\mathrm{B}}T}\right)\mathrm{d}E_{\mathrm{tr}}, \qquad (3)$$

where $x = (\mathrm{r},\ \mathrm{nr},\ \mathrm{total})$, $g_{\mathrm{e}} = [1 + \exp(-205/T)]^{-1}$ is the factor that accounts for the electronic degeneracies in the title reaction, k_{B} is the Boltzmann constant, μ is the reduced mass of the colliding particles, and T is the temperature (of course, the superscript 'total' refers to the sum of reactive and non-reactive events).

4. Results and discussion

Table 1 summarizes the trajectory calculations for $v = 6$ and 9, since the results for $v = 0 \rightarrow 4$ have been reported elsewhere [23,25]. Note that the number of reactive trajectories leading to the various channels are indicated separately in columns five to seven, while column eight gives the number of non-reactive trajectories leading to V–T energy transfer. To count these, we have first defined the v-state bin as encompassing the range $(E_v - E_{v-1})/2 \rightarrow (E_{v+1} - E_v)/2$, and considered as non-reactive V–T trajectories all those whose vibrational energy of OH fell outside that bin. We emphasize that this analysis is based on $b_{\max}$ values which have been calibrated for the reactive process. However, for testing their reliability, we have carried out two batches of trajectories for $v = 6$ and 9 at $E_{\mathrm{tr}} = 8$ kcal mol^{-1} in which $b_{\max}$ was optimized for non-reactive collisions. For this optimization, we have run batches of 100 trajectories at fixed values of b, and looked at the difference between the initial internal energy of the reactants and the average internal energy of the products for non-reactive collisions: $b_{\max}$ was then chosen as the smallest value of b for which such a difference fell within the numerical accuracy achieved in conserving the total energy. The calculated cross-sections using these two $b_{\max}$ values (denoted in an obvious correspondence with the superscripts r and nr) are gathered in Table 2. The agreement is satisfactory, and hence it may be concluded that the values reported in Table 1 are reliable.

Table 2
Comparison of $OH(v) + O_3$ reactive and non-reactive cross-sections calculated using b_{max} values which have been obtained from the analysis of reactive and non-reactive processes separately

v	b^{r}_{max} (a_0)	$\sigma^{r} \pm \Delta\sigma^{r}$ (a_0^2)	$\sigma^{nr} \pm \Delta\sigma^{nr}$ (a_0^2)	b^{nr}_{max} (a_0)	$\sigma^{r} \pm \Delta\sigma^{r}$ (a_0^2)	$\sigma^{nr} \pm \Delta\sigma^{nr}$ (a_0^2)
6	7.75	22.82 ± 1.94	10.75 ± 1.38	9.45	19.07 ± 2.23	10.66 ± 1.70
9	8.32	33.88 ± 1.44	26.93 ± 1.31	13.23	25.29 ± 3.64	25.84 ± 3.68

For completeness, the results obtained in previous work for $v = 0 \rightarrow 4$ [23,25] are also gathered in Fig. 2. Thus, we examine here the major trends involved in the whole series of studied vibrational states. First, we discuss HO_2 formation alone, which exhibits two types of regimes. (Since the resulting excitation functions σ^{r} vs E_{tr} are very similar in shape to those shown in Fig. 2, we omit them for brevity). The first arises for low translational energies, and corresponds to HO_2 formation via a capture-type mechanism where long-range forces play an important role. The second regime occurs for higher translational energies, and is more typical of a reaction with a threshold energy. Note that $OH(v)$ has increased electric dipole and quadrupole moments for the v states of interest in this work, which may explain the important role of long-range forces at low E_{tr} values. In turn, for increasing translational energies, the decrease of reactivity may be explained from the overlap of the electronic densities of the interacting species which is likely to lead on an average to an increase of the repulsive forces. Of course, the middle range of translational energies reflects the balance of such extreme behaviors.

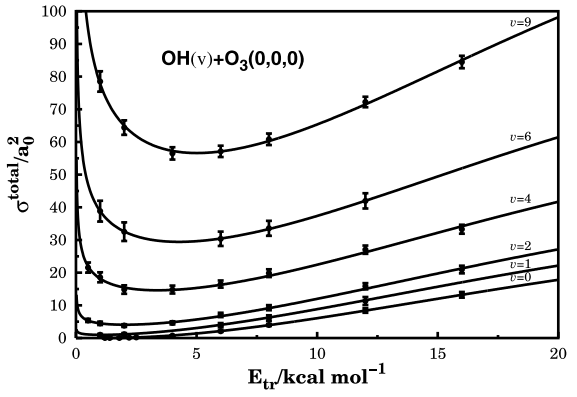

Fig. 2. Total cross-sections σ^{r} for quenching of $OH(v)$ as a function of the translational energy. Also indicated are the 68% error bars and the fitted model excitation function given by Eq. (4).

Table 3 shows the product's energy distribution for OH ($v = 6, 9$). As shown, the outcoming HO_2 molecules have a considerable internal energy content, with a significant part of it being in the rotational degrees of freedom. Thus, part of the translational and vibrational energies in the reactants has been converted to rotational energy in the products. The notable feature is perhaps the fact that the average value of the vibrational energy of the HO_2 radical represents more than half of the total energy of the products. Clearly, the product's internal energy is mostly channeled into the vibration of HO_2. Note that the average vibrational energy of HO_2 is much higher than the corresponding ZPE (8.5 kcal mol^{-1}). In fact, for $v \geqslant 6$, many HO_2 molecules end up with vibrational excitations above the dissociation limit. (These species, hereafter denoted $HO_2^{\star}$, might then be best catalogued under the headings diatom + diatom + atom. Since this has no implications on the total reactive cross-section, we make no attempt here to pursue their analysis further.) Although one might think that ZPE leakage ([27–33], and references therein) could therefore be safely ignored, this is not the case if the ZPE requirement is simultaneously imposed in the vibrational energy of the formed $HO_2^{\star}$ and O_2 molecules (vibrational energy quantum mechanical threshold (VEQMT) scheme [26]). Such a difficulty gets compounded for the higher product channels $O_2 + O_2 + H$ and $O_2 + OH + O$, where the requirement of both product molecules having at least ZPE is even more difficult to get satisfied. Another non-active scheme [26] would be to require the internal energy of each product molecule to be larger than or equal to its ZPE (internal energy quantum mechanical threshold (IEQMT)

Table 3
Average energies, and percentages of energy partitioned among different degrees of freedom for the reaction $OH(v) + O_3 \rightarrow HO_2^{\star} + O_2$[a]

v	E_{tr}	$\langle E_{tr}\rangle$	$\langle E_{tr}\rangle$	$HO_2^{\star}$				O_2			
			(%)	$\langle E_v\rangle$	$\langle E_v\rangle$ (%)	$\langle E_r\rangle$	$\langle E_r\rangle$ (%)	$\langle E_v\rangle$	$\langle E_v\rangle$ (%)	$\langle E_r\rangle$	$\langle E_r\rangle$ (%)
6	1.0	25.31	23.5	64.66	60.0	13.30	12.3	1.22	1.1	3.20	2.9
	2.0	27.15	25.0	60.75	55.8	16.36	15.0	1.43	1.3	3.09	2.8
	6.0	30.56	27.1	61.65	54.7	15.01	13.3	1.12	1.0	4.40	3.9
	8.0	28.83	25.1	64.87	56.5	15.78	13.7	1.11	1.0	4.14	3.6
	12.0	33.40	28.1	63.04	53.1	17.06	14.4	1.32	1.1	3.88	3.3
9	1.0	32.60	25.4	74.45	58.1	14.59	11.4	1.31	1.0	5.27	4.1
	2.0	32.17	24.9	76.64	59.3	15.32	11.8	1.13	0.9	3.96	3.1
	4.0	37.53	28.6	68.88	52.5	18.94	14.4	1.32	1.0	4.50	3.4
	6.0	34.45	25.9	73.75	55.4	17.77	13.3	1.04	0.8	6.16	4.6
	8.0	34.55	25.6	76.50	56.6	16.70	12.4	1.63	1.2	5.70	4.2
	12.0	42.20	30.3	69.45	49.9	19.98	14.4	1.33	1.0	6.16	4.4
	16.0	41.47	30.0	75.51	52.8	19.53	13.7	1.37	1.0	5.15	3.6

[a] Energies are given in kcal mol^{-1}.

scheme [26]). Clearly, VEQMT is more demanding than IEQMT, and is perhaps too restrictive [26,28] (such a restrictive nature of VEQMT gets enhanced when two or more molecules are formed). A softer usage of it might be to require that the total vibrational energy in the products is larger than the sum of ZPEs in the product molecules. In fact, since there is a continuous flow of vibrational energy, one would avoid the arbitrariness of picking the moment at which the products are considered as formed. Thus, we have also compared the vibrational energy and ZPE of the complex just prior to product formation (this is reported in Table 4 under the heading $VEQMT_C$), assuming that the required quantities can be extracted from the separated species. As seen from Table 4 (see also Table 1), the results show drastic differences. However, it is reassuring that $VEQMT_C$ supports the QCT results. Of course, for consistency, one should also mind the fate of non-reactive trajectories. We have looked at the energy distributions of O_3 (OH is always vibrationally hot) in such trajectories for $v = 6, 9$, and observed the following: for $v = 6$, the average vibrational energy of O_3 is, for all translational energies except $E_{tr} = 1.0$ kcal mol^{-1}, slightly above ZPE (4.2 kcal mol^{-1}); for $v = 9$, such an average value tends to be slightly below ZPE for all values of E_{tr} except $E_{tr} = 16$ kcal mol^{-1}. In summary, since there is no unambiguous way to fix the ZPE leakage problem of classical mechanics (the only solution is via quantum mechanics), we use the QCT results in the subsequent analysis.

Finally, we examine the shape of the excitation functions for reactive scattering (formation of $HO_2^{\star} + O_2$, $OH + O_2 + O$, and $O_2 + O_2 + H$) and total quenching of $OH(v)$ (both reactive and non-reactive). Since their shapes differ only quantitatively, we show only the curves for total quenching of $OH(v)$ in Fig. 2, together with the associated 68% error bars. Besides the new cross-sections for $v = 6, 9$, we include also the results reported elsewhere [23,25] for $v = 0 \rightarrow 4$. We emphasize that two opposite trends explain their shape: a capture-type regime [34,35] dominates at low energies while a pattern common to reactions having an energy threshold is favored at high energies. Their balance can be well described by the following model excitation function:

$$\sigma^{x}(E_{tr}, v) = \frac{\sum_{i=1}^{3} c_i v^i}{E_{tr}^{n}} + \left(\sum_{j=0}^{3} d_j v^j\right)\left[E_{tr} - E_{tr}^{th}(v)\right]^{\tilde{n}} \times \exp\left\{-m\left[E_{tr} - E_{tr}^{th}(v)\right]\right\}, \quad (4)$$

where

$$E_{tr}^{th}(v) = 1.056\exp(-v/\alpha), \quad (5)$$

where $x = r$ and total have the meaning previously assigned. Note that the first term describes the v-dependent capture contribution of the

Table 4
A comparison of the number of reactive trajectories for the title reaction[a] according to the VEQMT[a], and IEQMT[b] schemes

v	E_{tr}	$HO_2^\star + O_2$			$O_2 + O_2 + H$			$O_2 + OH + O$		
		IEQMT	VEQMT$_C$	VEQMT	IEQMT	VEQMT$_C$	VEQMT	IEQMT	VEQMT$_C$	VEQMT
6	1.0	38	42	5	37	53	6	5	8	2
	2.0	34	40	10	34	43	6	5	10	1
	6.0	36	45	5	32	41	6	7	10	1
	8.0	39	52	8	35	42	6	6	12	2
	12.0	51	65	13	55	71	10	16	19	2
9	1.0	31	40	9	167	228	17	46	62	13
	2.0	50	69	6	213	249	35	66	78	15
	4.0	56	69	12	213	257	36	41	53	11
	6.0	50	75	8	203	267	44	56	72	12
	8.0	63	75	20	254	291	45	51	70	11
	12.0	86	104	15	345	420	68	98	105	23
	16.0	75	90	15	273	333	48	66	77	15

[a] For the pure QCT values, see Table 1.
[b] From [26].

cross-section, while the second term represents the threshold-energy-type component (which includes also a dependence on the vibrational quantum number of OH). Note further that the threshold energy contains a rapidly decaying dependence on v, as suggested by the near-absence of an energy threshold for values of $v \geqslant 1$. Except for the parameter α, which has been optimized by trial-and-error, all others have been determined from a least-squares fitting procedure to the ($v = 0 \rightarrow 9$) calculated data. The optimum numerical coefficients are given in column two of Table 5; units are such that when the energy is in kcal mol^{-1}, the cross-section is in a_0^2. Also shown is the form in Eq. (4), which is seen to fit very well the calculated points. In particular, the data for $v = 0$ and $v = 1 \rightarrow 4$ are reproduced to an accuracy similar to that reported for the separate fits [23,25]. Similar considerations apply to the cross-sections for total quenching of OH(v); the corresponding parameters are also given in Table 5.

By substitution of Eq. (4) in Eq. (3) and integrating analytically, one gets

$$k_v^x(T) = g_e(T)\left(\frac{8}{\pi\mu}\right)^{1/2}\left\{\left(\sum_{i=1}^{3} c_i v^i\right) \times \Gamma(2-n)(RT)^{-n+1/2} + \left(\sum_{i=0}^{3} d_i v^i\right)\frac{(RT)^{\tilde{n}+1/2}\exp\left[-E_{tr}^{th}(v)/RT\right]}{(1+mRT)^{\tilde{n}+2}} \times \left[\Gamma(\tilde{n}+2)+\Gamma(\tilde{n}+1)(1+mRT)E_{tr}^{th}(v)/RT\right]\right\}, \quad (6)$$

where $\Gamma(\cdots)$ is the gamma function, and all other symbols have their usual meaning. Fig. 3 shows as a perspective plot the calculated specific thermally averaged rate coefficients $k_v^{total}(T)$, while Fig. 4 shows a cut on the two-dimensional plot of Fig. 3 for $T = 300$ K. The notable feature from Fig. 4 is the drastic change in the temperature dependence for different v values. Note that the dashed curve crosses the solid one at $v \sim 3$, which has no physical meaning due to being within the uncertainties associated to the independently fitted data. Clearly, the rate constant for $v = 0$ increases with T, while those for high values of v show only a

Table 5
Numerical values of coefficients in Eq. (6)

Coefficient	σ^{r}	σ^{total}
c_1	−0.54129(0)[a]	−0.52375(0)
c_2	1.52151(0)	1.44931(0)
c_3	−0.85993(−1)	−0.48158(−1)
d_0	0.96698(−1)	0.95326(−1)
d_1	0.14459(−1)	0.01276(0)
d_2	−0.42591(−3)	−0.16244(−2)
d_3	−0.47827(−5)	−0.20453(−4)
n	0.40728(0)	0.28371(0)
$\tilde{n}$	2.09519(0)	2.10079(0)
m	0.5(−1)	0.5(−1)
α	0.1(0)	0.1(0)

[a] Powers of ten are given in brackets.

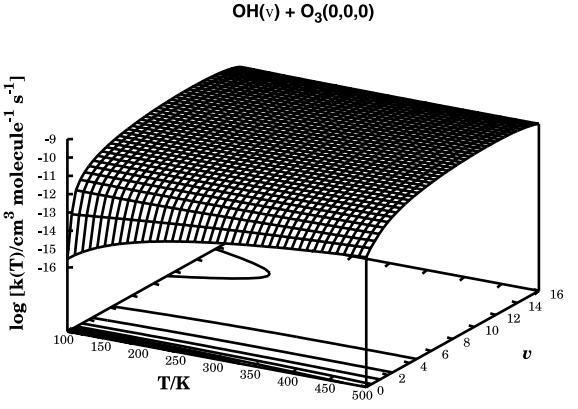

Fig. 3. Total (reactive plus non-reactive) thermal rate coefficient for $OH(v) + O_3$ as a function of temperature and vibrational quantum number of OH.

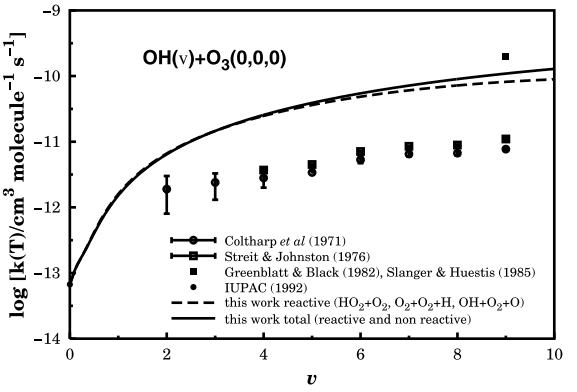

Fig. 4. A comparison of the total reactive and reactive plus non-reactive thermal rate coefficient for $OH(v) + O_3$ as a function of vibrational quantum number of OH for $T = 300$ K. Also indicated are the 68% error bars and the fitted line given by Eq. (6).

slight increase or even a slight decrease with T. These findings are in agreement with the fact that the reaction for $v = 0$ has a threshold energy while for high v values, it is dominated by a capture-type mechanism. Also visible is a broad maximum as a function of v, peaking nearly $v = 10$. Such a feature is plausible since the probability of forming $HO_2^{\star}$ is likely to decrease for excessively large values of v. However, the calculated rates extend only up to $v = 9$, and hence one should not overemphasize its importance. Finally, we observe from Fig. 4 the fairly good agreement between our calculated total rate constant for quenching of $OH(v = 9)$ at $T = 300$ K and the best available measurement [9,19].

5. Concluding remarks

We have reported a QCT study of the reaction $OH(v = 0 \rightarrow 9) + O_3$ using a recently published DMBE potential energy surface for ground state HO_4. The calculations have shown that the title reaction may occur both via capture-type and barrier-type mechanisms, depending on the reactant initial conditions, especially the degree of OH vibrational excitation. A comparison with experimental data for $v = 0, 9$ shows good agreement, and suggests that the title bimolecular collisions occur mostly via a chemical reaction. Due to difficulties in the earlier experimental measurements

and incorrect kinetic analysis, the comparison for intermediate v values is possibly meaningless. An estimate of non-reactive quenching has also been given for the title collisional process, although a quantitative answer must await the use of semi-classical or quantum methods. In any case, a comparison with the non-reactive rates calculated by Teitelbaum et al. [18] leads us to conclude that reactive scattering cannot be discarded, and is even dominant over non-reactive scattering for the HO_4 DMBE potential energy surface.

Acknowledgements

The support of Fundação para a Ciência e Tecnologia, Portugal, under programme PRAXIS XXI is gratefully acknowledged.

References

[1] D.R. Bates, M. Nicolet, J. Geophys. Res. 55 (1950) 301.
[2] A.B. Meinel, Astrophys. J. 112 (1950) 120.
[3] G. Herzberg, J. R. Astron. Soc. Can. 45 (1951) 100.
[4] D.V. Shalashilin, A.V. Michtchenko, S. Umanskii, Y.M. Gershenzo, J. Phys. Chem. 99 (1995) 11627.
[5] J.I. Steinfeld, S.M. Adler-Golden, J.W. Gallagher, J. Phys. Chem. Ref. Data 16 (1987) 911.
[6] P.J.S.B. Caridade, L. Zhang, J.D. Garrido, A.J.C. Varandas, J. Phys. Chem. A (in press).
[7] A.J.C. Varandas, P.J.S.B. Caridade, Chem. Phys. Lett. (in press).
[8] B.J. Finlayson-Pitts, T.E. Kleindienst, J. Chem. Phys. 74 (1981) 5643.
[9] G.D. Greenblatt, J.R. Wiesenfeld, J. Geophys. Res. 87 (1982) 11145.
[10] D.V. Shalashilin, S.Y. Umanskii, Y.M. Gershenzon, Chem. Phys. 168 (1992) 315.
[11] K.J. Rensberger, J.B. Jeffries, D.R. Crosley, J. Chem. Phys. 90 (1989) 2174.
[12] G.A. Raiche, J.B. Jeffries, K.J. Rensberger, D.R. Crosley, J. Chem. Phys. 92 (1990) 7258.
[13] A.D. Sappey, R.A. Copeland, J. Chem. Phys. 93 (1990) 5741.
[14] J.A. Dodd, S.J. Lipson, W.A.M. Blumberg, J. Chem. Phys. 95 (1991) 5752.
[15] B.R. Chalamala, R.A. Copeland, J. Chem. Phys. 99 (1993) 5807.
[16] K. Knutsen, M.J. Dyer, R.A. Copeland, J. Chem. Phys. 104 (1996) 5798.
[17] C. Zhurt, L. Zülicke, S.Y. Umansky, Chem. Phys. 105 (1986) 15.
[18] H. Teitelbaum, P. Aker, J.J. Sloan, Chem. Phys. 119 (1988) 79.
[19] R. Atkinson, D.L. Baulch, R.A. Cox, R.F. Hampson Jr., J.A. Kerr, J. Troe, J. Phys. Chem. Ref. Data 21 (1992) 1125.
[20] R.N. Coltharp, S.D. Worley, A.E. Potter Jr., Appl. Opt. 10 (1971) 1786.
[21] T.G. Slanger, D.L. Huestis, Int. J. Chem. Kinet. 17 (1985) 713.
[22] T.G. Slanger, R.A. Copeland, Current Problems and Progress in Atmospheric Chemistry, World Scientific, Singapore, 1996.
[23] A.J.C. Varandas, L. Zhang, Chem. Phys. Lett. 331 (2000) 474.
[24] W.L. Hase, R.J. Duchovic, X. Hu, A. Komornicki, K.F. Lim, D. Lu, G.H. Peslherbe, K.N. Swamy, S.R.V. Linde, A.J.C. Varandas, H. Wang, R.J. Wolf, QCPE Bull. (1996) 43.
[25] L. Zhang, A.J.C. Varandas, Phys. Chem. Chem. Phys. 3 (2001) 1439.
[26] A.J.C. Varandas, J. Chem. Phys. 99 (1993) 1076.
[27] A.J.C. Varandas, Chem. Phys. Lett. 225 (1994) 18.
[28] A.J.C. Varandas, J.M.C. Marques, J. Chem. Phys. 100 (1994) 1908.
[29] S. Kumar, N. Sathyamurthy, R. Ramaswamy, J. Chem. Phys. 103 (1995) 6021.
[30] M. Ben-Nun, R.D. Levine, J. Chem. Phys. 105 (1996) 8136.
[31] Y. Guo, D.L. Thompson, T.D. Sewell, J. Chem. Phys. 104 (1996) 576.
[32] K.F. Lim, J. Chem. Soc. Faraday Trans. 93 (1997) 669.
[33] A.J. Marks, J. Chem. Phys. 108 (1998) 1438.
[34] W. Wang, R. González-Jonte, A.J.C. Varandas, J. Phys. Chem. 102 (1998) 6935.
[35] A.J.C. Varandas, Faraday Discuss. Chem. Soc. 84 (1987) 353.